DOI 10.59277/RoAJ.2023.3.02

# NEW ASTRO-GEODETIC MEASUREMENTS FOR GEOID MODELING

ALEXANDRU CĂLIN[1], PAUL DANIEL DUMITRU[1], OCTAVIAN BĂDESCU[2], ADRIAN SAVU[1]

[1] *Technical University of Civil Engineering, Faculty of Geodesy*
*Bd. Lacul Tei 124, Bucharest, Romania*
E-mail: *alexandru.calin@utcb.ro, paul.dumitru@utcb.ro, adrian.savu@utcb.ro*

[2] *Astronomical Institute of the Romanian Academy*
*Str. Cuţitul de Argint 5, 040558 Bucharest, Romania*
E-mail: *octavian.badescu@astro.ro*

*Abstract*. The paper presents the results obtained in four points regarding the astro-geodetic vertical deviation determination. The four points located in the metropolitan area of Bucharest city and they are stationed twice, in 2015 and 2023. Observations were realized by a platform composed by an electronic total station coupling with a micro-CCD camera and a GPS time receiver, all controlled by a portable PC. For every station were realized more sessions of observations in both years. For vertical deviation calculus we used geodetic coordinates extracted from models, while astronomical coordinates were measured in the field. The goal of these astro-geodetic determinations is to serve for testing and evaluating global geoid models as EGM2008 and GOCE, as well as to validate the historical astro-geodetic determinations in our country.

*Key words:* astrometry, geodesy, CCD, vertical deviation.

## 1. INTRODUCTION

Astro-geodetic observations represent the combination of two different approaches regarding positioning on the Earth surface. Astronomical observations basically mean ground astrometry with adequate instruments for as precise and accurate as possible determination of the observation point position on the Earth's topographical surface. The result of astronomical the observations is the latitude $\Phi$ and longitude $\Lambda$ , called astronomical coordinates, in accordance with the name of the determination method. The second approach for positioning is by geodetic techniques which provide, for the same point on the Earth's surface the second coordinates set called geodetic latitude $\phi$ and longitude $\lambda$. The geodetic positioning implies either geodetic terrestrial measurements or satellite/GNSS (Global Navigation Satellite System) determinations. So, in the same point on the Earth's surface we have two different coordinates pairs: ($\Phi$ , $\Lambda$ ) and ($\phi$ , $\lambda$ ).

In present, several long–wave global geoid models (smooth surfaces) are developed and mainly serve as reference for a better global or zonal geoid model. The combination between the global models augmented by local and regional data from terrestrial measurements is a suitable solution for obtaining a high-resolution geoid. Terrestrial methods as the astro-geodetic one are able to detect short wavelength structures of the geoid beside gravimetric, GNSS (Global Navigation Satellite System) and levelling methods. All these terrestrial methods have both advantages and disadvantages, general rule being their common use. Despite the well-known difficulties in obtaining, one of the most valuable quantities used for geoid determination or geoid modelling is the Helmert astro-geodetic vertical deviation (v.d.). Helmert v.d. is considered "… *rich in high-frequency gravitational information, observed values of the astronomic (or Helmert) deflections are well suited to assess the high-degree spectrum of a geopotential model*" (Jekeli, 1999), and for this reason is used in several exhaustive studies concerning validation of the global geoid models as GOCE (Gravity field and steady-state Ocean Circulation Explorer) or EGM2008 (Earth Gravitational Model 2008). At the international level, there are some ongoing projects, the geoid problem, both at global level or regional level being an actual problem of geodesy (Featherstone W.E. and Morgan L., 2007; Hirt C., et al., 2010b; Voigt C. and Denker H., 2011).

## 2. INSTRUMENTS

As already described in our previous paper (Bădescu, O., et al, 2015, 2016a, 2010) the measuring platform is composed by a geodetic total station for precise angular measurement (Topcon MS05AX, 168 mm telescope length, 45 mm telescope aperture, $30\times$ telescope magnification, $0''.1$ minimum angular value displayed, $0''.5$ angular accuracy, with tilt angle compensator and 5 brightness levels for reticle illumination) to which was attached a small CCD camera (XIMEA MU9PM-MH, resolution 5MP, 2592×1944 pixels, sensor size 5.70×4.28 mm, pixel 2.2×2.2 μm, 20 μs–500 s) for automate determination of the intersection time of the star trajectory with the reticular wires of the total station telescope. A small GPS receiver ensures the time base for the time measurements and astrometric computations. The entire platform, including de observational process and the data adjustment is controlled by a laptop, thus the components $\xi$ (meridian) and $\eta$ (prime vertical) of the deviation of the vertical are obtained right after the observations are completed.

A time-based GPS receiver was built on a dedicated, modular Raspberry PI V3

Model B micro-computer and a Neo 6M v2 GPS receiver, with NMEA and PPS capabilities, connected to the motherboard of the micro-computer. The control and command of this time and position receiver is done via a web interface that permanently provides device status as well as synchronization and positioning details (Figure 1).

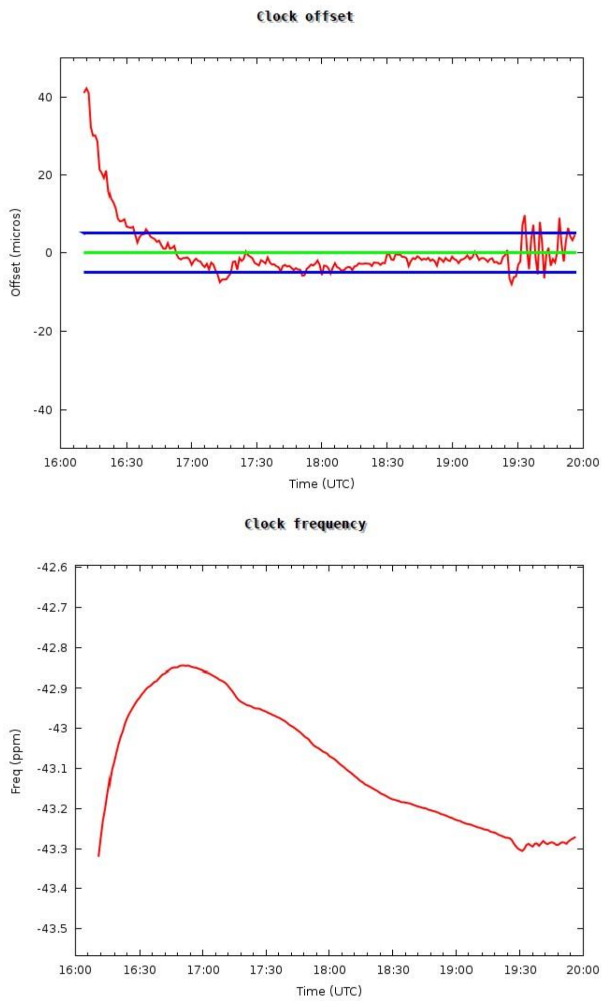


Fig. 1 – Clock offset and frequency during the observation session at 27.06.2023. *In situ* these parameters are observed permanently. In the case of some abnormal offset (over ± 5 microseconds) measurements are eventually interrupted.

The dedicated software for astro-geodetic measurements has a several characteristics, for using with a geodetic total station gifted by a CCD camera and the GPS time receiver, all being coupled on a portable PC. All components are connected to and controlled by the portable PC (Bădescu, O., et al, 2015, 2016a, 2010):

- Runs under Linux – Ubuntu operating system;
- Generate virtual reticular wires which can be translated on any direction and rotate (in step of 0.1 pixel for translations and 0.1 degree for rotation, or so-called auto-wire function);
- Ensures the time measurement by synchronizing with the external GPS time receiver via LAN port;
- It has functions for obtaining quality images – astrometric images, as: setting the time interval between consecutive images, gain, exposure time, image scale and detection sigma, create a master dark;
- Allow introduction of the star name, angular measurements from the geodetic instrument (azimuth and zenithal distance) as well as the atmospheric parameters (pressure, temperature and humidity), measured at the beginning or at the end of observations;
- No image is stored in the computer (acquisitions data laptop);
- At the end of the observations for every star separately provide the time of intersection with the virtual reticular wires (previously overlapped on the real reticular wires). Also, it is providing the image of the calculated trajectory and rms (root mean square) of the fitting (fitrms);
- Create a file which contain for each observed star, angular values and corresponding times, atmospheric parameters, images number and the fitrms of the trajectory fitting using star centroids separately for azimuthal and zenithal measurements;
- At the software application has been used ESO CPL (European Southern Observatory Common Pipeline Library), GTK (Graphic Toolkit) for interface and XIMEA SDK (Software Development Kit).

## 3. DATA AQUISITION

Astro-geodetic observations were made in four different locations from Bucharest city area and it's surroundings (Figure 2). Two locations are inside of the Bucharest city (AIRA – Astronomical Institute of the Romanian Academy and HTL – Hydro Technical Laboratory of the Bucharest Technical University of Civil Engineering), gifted by pilaster with forced centering and for other two, situated on the Bucharest ring road, observations were performed on the tripod of the total station (E – East and SE – South East). In addition, both locations inside Bucharest city area show obstructions in certain directions, such as buildings or tall trees, thus unable to ensure a quite uniform azimuthal distribution of the observed stars. Lines of sight which pass over the buildings are affected by parasitic refractions caused by the warmer air around them. However, all the stations are relative improperly for astronomical (astrometric) observations, being affected by atmospheric and light pollution, characteristics of urban areas, or relative instability caused by using the tripod (Figure 3).

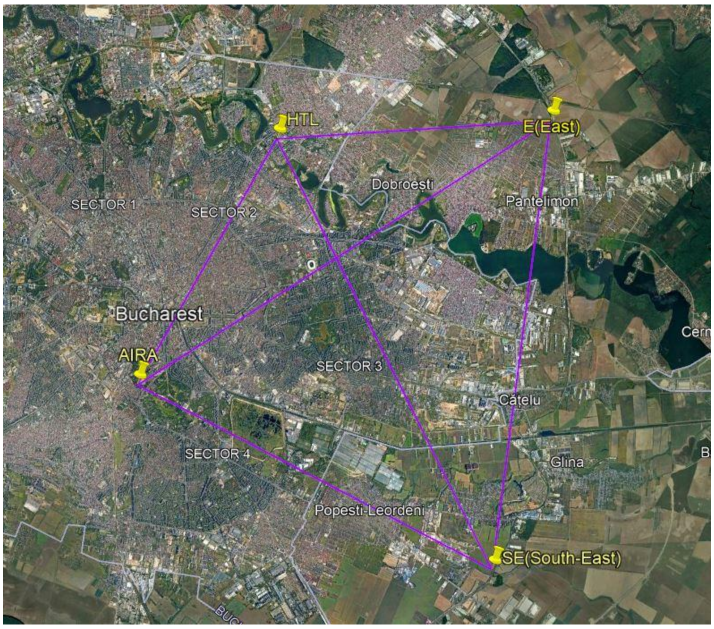


Fig. 2 – Four astro-geodetic points on the Bucharest area: AIRA, HTL, E and SE. Approximative distance from points are: AIRA-HTL ~ 7.2 km, HTL-E ~ 7.1 km, E-SE ~ 11.7 km, SE-AIRA ~ 10.36 km and diagonals HTL-SE ~ 12.4 km and AIRA-E ~ 12.7 km.

All observations were made in both positions of the total station's telescope (Face 1 – Face 2) to limit residual instrumental errors and for every star the atmospheric parameters (pressure, temperature and humidity) were taken at the middle of the timing of observations. Every star was observed both azimuthal and zenithal. In some nights, the sequence Face 1 – Face 2 was replaced by Face 1 – Face 2 / Face 2 – Face 1 or Face 1 – Face 2 / Face 2 – Face 1 / Face 1 – Face 2 meaning a doubling or tripling the number of measurements for each observed star.

Every observed star generates 2 equations, one corresponding to the azimuthal observations and the second corresponding to the zenithal observations. So, for $n$ observed stars, at least in the sequence Face 1 – Face 2, we will have $n \times 2$ equations.

For every observation night we aimed at achieving a uniform azimuthal distribution of the observed stars. These measurements were processed by a functional stochastic model based on the theory of conditional measurements with unknowns. Least square adjustment was used to find the unknowns of the models, that is astronomical latitude, longitude and azimuth of the station point (the last one is an additional result, unused for vertical deviation determination). Based on the measurement corrections (angular and time measurement) obtained after the least square adjustment, two statistical tests were used to eliminate the measurements considered erroneous.


Fig. 3 – Three stationed astro-geodetic points: left figure, HTL (pilaster, forced centering); center figure, AIRA (pilaster, forced centering) and right figure, the E station (stationed on the tripod of the total station).

According to the star apparent motion in the optical field (trajectory relative to the crosshairs and apparent speed), the number of the images captured for every observed star has varied from a few dozen to a few hundred. For every observed star, the exposure time varied according to the atmospheric conditions and the stars' magnitude (brightness), and the time interval between two consecutive images varied according to the apparent motion in the optical field. In general, for all of the observed stars it was intended that the trajectory passes as close as possible to the intersection of the crosshairs, symmetrical to this point and as short as possible (Figure 4, Figure 5).

Besides the angular values taken from the total station, the atmospheric parameters (pressure in mbar, temperature in $^{o}$C and relative humidity in %) are introduced manually. All these parameters are written into a file data (Table 1). In Figure 5, left image, follow by right image, come from a Face 2 – Face 1 sequence, from $21^{h}22^{m}42^{s}.309$ to $21^{h}25^{m}30^{s}.457$, which means approximative 3 minutes. The entire period of Face 2 – Face 1 sequences hold maximum 5-6 minutes.

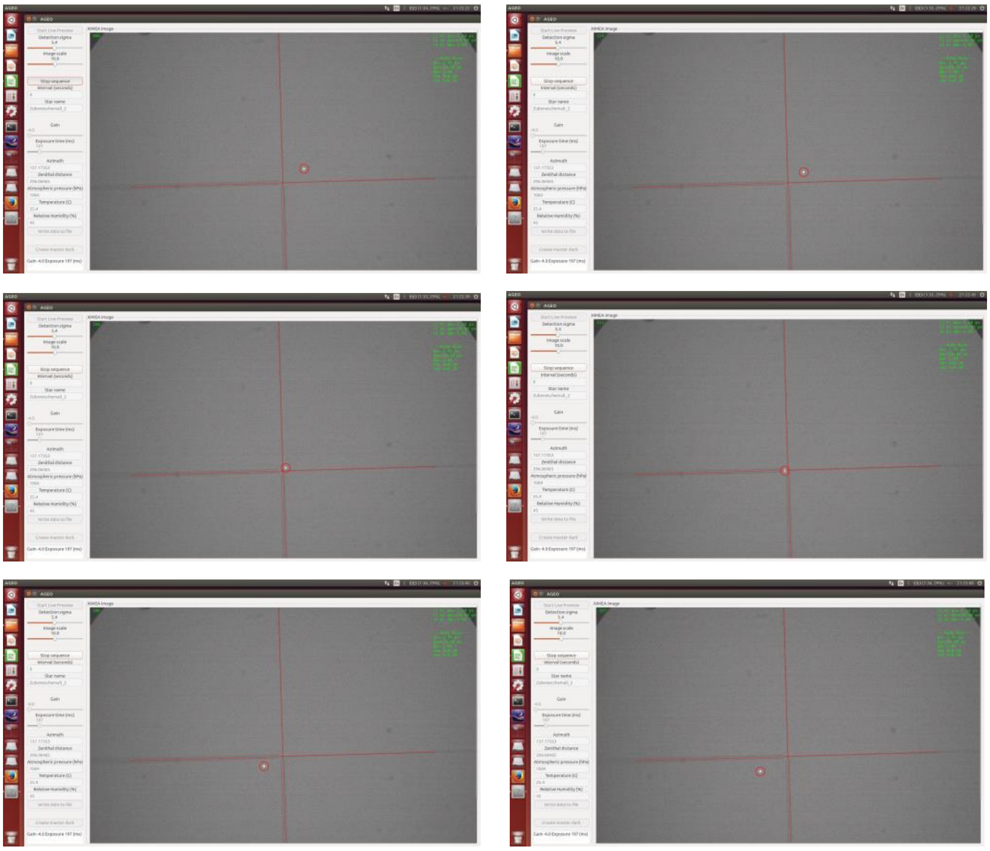

Fig. 4 – Six consecutive images random taken from almost 500 ones, for the star Zubeneschamali (Beta Librae, Absolute magnitude -1.16), in 21.06.2023, at AIRA station. The star trajectory is passing the reticular wires on diagonal and almost in the center (from the upper right corner to the lower left corner). The exposure time, as we can see in the images, was 197 ms and the interval from two consecutives images was 20 µs.

In this conditions, 10 stars could be observed under one hour. Both images from Figure 5 comes from 21.06.2023, for the star Zubeneschamali, Face 2 – Face 1.

Angular values of the azimuth and the zenithal distance, calculating times corresponding to the angular values (moments corresponding to the intersection of the star trajectory with the crosshairs) and the atmospheric parameters are saved in an observations file (Table 1).

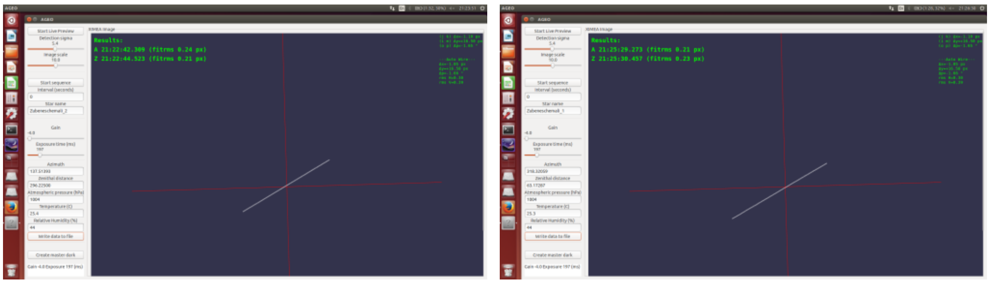

Fig. 5 – Times of crossing reticular wires, separately for vertical (A, azimuthal) and horizontal (Z, zenithal) wire and corresponding fitrms (in pixel) are automatically calculated by software. Angular values for azimuth and zenithal distance are taken from the total station. Both images come from a sequence Face 2 – Face 1 (Zubeneschamali 2 – Zubeneschamali 1), at AIRA station in 21.06.2023.

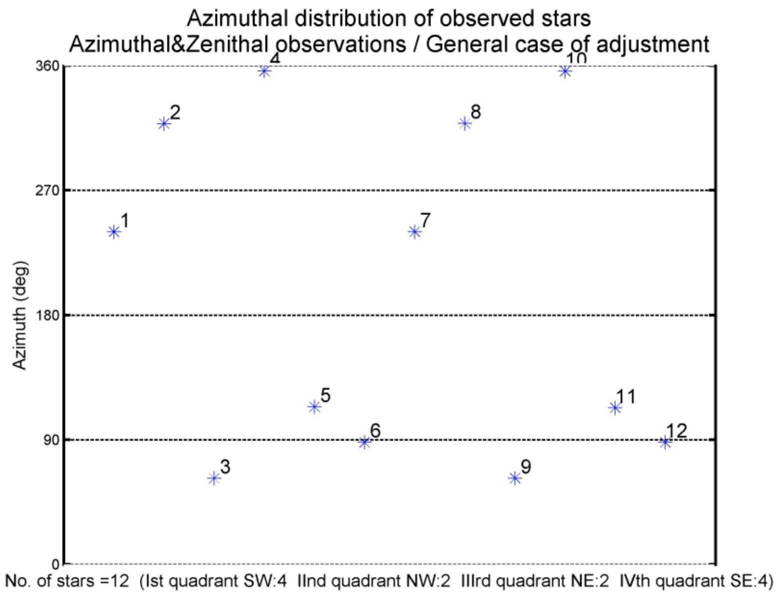


Fig. 6 – Azimuthal distribution of 12 observed stars in 21.06.2023. Each star marked on the above graphic come from a pair Face 1 – Face 2 or Face 2 – Face 1. Stars 2 and 8 is Zubeneschamali (twice observed Face 2 – Face 2 – Face 1 – Face 1), 1 and 7 is Vega, 3 and 9 Regulus and so on (see the Table 1).

Immediately after the observations are ended, the software application accesses the observations file and calculate the component of the vertical deviation and the total vertical deviation ($\xi$, $\eta$ and $\varepsilon$), as well as a graphic with the azimuthal distribution of the observed stars into a single session (Figure 6).

*Table 1*

Lines of data from an observations file (stars observed in the Face 1 – Face 1 – Face 2 – Face 2 sequences at the station AIRA at 21.06.2023)

21.06.2023

Passing clouds, visibility difficulties, different exposure times, reticular fires alignment verified, normal function of the GPS time receiver. From time to time, wind blowing. At the end of the night observation, the sky was totally covered by clouds, so the azimuthal uniform distribution was affected (for instance, Errai, the final observed star, it could no longer be observed in the Face 2 position). Some stars were observed through clouds.

002 Vega_1 239.36459[1] 64.33122[2] 1004.0[3] 25.6[4] 43.0[5] 21.0839059[6] 0.21[7] 416[8] 21.0838939[9] 0.27[10] 416[11]
003 Vega_1 239.57131 64.09571 1004.0 25.6 43.0 21.1113969 0.16 413 21.1109290 0.21 413
004 Vega_2 60.17179 296.14505 1004.0 25.5 43.0 21.1346210 0.15 404 21.1348835 0.19 404
005 Vega_2 60.34478 296.34393 1004.0 25.5 43.0 21.1559067 0.19 419 21.1556131 0.22 419

006 Zubeneschemali_2 137.17353 296.06465 1004.0 25.4 43.0 21.2020666 0.23 517 21.2031337 0.22 517
007 Zubeneschemali_2 137.51393 296.22500 1004.0 25.4 44.0 21.2242309 0.24 401 21.2244522 0.21 401
008 Zubeneschemali_1 318.32059 63.17287 1004.0 25.3 44.0 21.2529272 0.21 435 21.2530456 0.23 435
009 Zubeneschemali_1 318.58331 63.03153 1005.0 25.3 44.0 21.2717902 0.22 511 21.2731038 0.22 511
010 Zubeneschemali_1 319.21373 62.53102 1005.0 25.3 44.0 21.2852357 0.24 456 21.2857186 0.22 456

011 Regulus_1 61.10101 48.29192 1005.0 25.2 44.0 21.3237163 0.21 457 21.3239073 0.23 457
012 Regulus_1 61.42035 48.48577 1005.0 25.1 44.0 21.3444424 0.20 403 21.3443833 0.21 403
013 Regulus_2 242.23271 310.45100 1005.0 25.0 45.0 21.3731284 0.21 404 21.3727942 0.21 404
014 Regulus_2 242.54280 310.24545 1005.0 25.0 45.0 21.3937547 0.22 405 21.3935279 0.23 405

015 Spica_2 175.14552 304.13519 1005.0 24.7 45.0 21.4500137 0.23 408 21.4446646 0.27 408
016 Spica_2 175.50020 304.15279 1005.0 24.7 45.0 21.4658383 0.20 408 21.4639277 0.20 408
017 Spica_1 356.34024 55.42357 1005.0 24.5 46.0 21.4926299 0.21 407 21.4927852 0.21 407
018 Spica_1 357.06133 55.41360 1005.0 24.6 46.0 21.5114569 0.22 409 21.5106887 0.22 409

019 Castor_1 112.15214 66.26240 1005.0 24.3 46.0 21.5907253 0.24 455 21.5913372 0.24 455
020 Castor_1 113.00231 67.18226 1005.0 24.1 47.0 22.0415651 0.26 405 22.0428259 0.28 405
021 Castor_1 113.21038 67.38197 1005.0 24.1 47.0 22.0637139 0.26 454 22.0629748 0.32 454
022 Castor_2 293.45033 291.56031 1005.0 24.0 47.0 22.0921027 0.28 508 22.0906352 0.30 508
023 Castor_2 293.57053 291.39537 1005.0 23.8 48.0 22.1043181 0.28 456 22.1045354 0.37 456
024 Castor_2 294.15020 291.18537 1005.0 23.9 47.0 22.1245731 0.26 425 22.1254011 0.35 425

025 EpsLeo_2 267.18307 307.46152 1005.0 23.7 48.0 22.2006863 0.26 404 22.1958700 0.30 404
026 EpsLeo_2 267.41027 307.23247 1005.0 23.7 48.0 22.2211006 0.30 416 22.2206398 0.32 416
027 EpsLeo_1 88.04094 52.59000 1005.0 23.6 48.0 22.2418790 0.35 478 22.2411506 0.44 478
028 EpsLeo_1 88.19414 53.14524 1005.0 23.6 48.0 22.2545230 0.28 432 22.2540320 0.32 432
029 EpsLeo_1 88.42140 53.39148 1005.0 23.5 48.0 22.2751233 0.25 422 22.2756575 0.28 422

030 Errai_1 188.22360 56.00122 1005.0 23.4 47.0 22.3331125 0.53 311 22.3303369 0.40 311
031 Errai_1 188.32401 55.54572 1005.0 23.4 47.0 22.3631066 0.25 628 22.3623798 0.30 628
032 Errai_1 188.37520 55.52424 1005.0 23.3 47.0 22.3804501 0.27 456 22.3747578 0.29 456

Explanation for Table 1 (Călin, A., et al, 2018): [1] Azimuthal angular value of the observed star, taken from the total station. [2] Zenithal angular value (zenithal distance) of the observed star, taken from the total station. (3) Atmospheric pressure. (4) Atmospheric temperature. (5) Atmospheric humidity. (6) Time corresponding to the azimuthal angular value of the observed star (the moment of the star's crossing to the vertical reticular wire) in the Coordinated Universal Time scale (UTC). (7) The root mean square of a two-degree polynomial trajectory fitted on the star centroids from every captured image, for calculating the intersection time with the vertical reticular wire (azimuthal observation). Represent a measure of the quality for azimuthal observations. (8) The number of images used to calculate the trajectory and the intersection moment with the vertical reticular wire (azimuthal measurements). (9) Time corresponding to the zenithal angular value of the observed star (the moment of the star's crossing to the horizontal reticular wire) in the Coordinated Universal Time scale (UTC). (10) The root mean square of a two-degree polynomial trajectory fitted on the star centroids for the intersection with the horizontal reticular wire (zenithal observation). Represent a measure of the quality for zenithal observations. (11) The number of images used to calculate the trajectory and the intersection moment with the horizontal reticular wire (zenithal measurements).

## 4. RESULTS

As already mentioned, currently, CCD technology become a key element in the astro-geodetic determinations. In the last decade, significant results were obtained by developing new instruments for astro-geodetic determinations, mostly based on zenithal cameras (former photographic zenithal tubes). These instruments have more features, among which we can mention it: do not need horizontal orientation, astronomical refraction has little influence near the zenith and are transportable (Bürki B., et al., 2007; Hirt, C., et al, 2002, 2004, 2010a).

All four points were stationed twice. First, during 2015 inside of the incipient test when the equipment’s of astro-geodetic platform was purchased and assembled and second, in 2023, after some improvements regarding software, observations technique, the clamping system of the micro-CCD camera and other.

Results obtained for the four mentioned points are presented in the Table 2. For every point was realized more sessions, in the same night, with a variable number of observed stars, both for the 2015 and 2023. For instance, the point HTL was observed in 15.07.2015, three times, using 18, 8 and 12 stars for each session. The same point was observed in 13.07.2023, twice, using 18 and 8 stars for each session. For all session, stars were observed at least in the sequences Face 1 – Face 2, or even more.

Deviation of the vertical using for control and comparations, meridian and prime vertical components too, come from Romanian historical astronomical observations realized by Topographical Military Directorate (DTM), GOCE spherical harmonic

*Table 2*

Values of deviations of the vertical resulting from CCD observations in the points HTL, E, SE and AIRA, during 2015 and 2023 comparative with values derived by interpolation from historical data (DTM), EGM2008 and GOCE global geoid models. $s_{(0)}$ standard deviation of a single series; $s_{(\xi)}$ standard deviation of the meridian component $\xi$, $s_{(\eta)}$ standard deviation of the prime vertical component $\eta$, all values expressed in arcseconds.

| Station/Data | No. of observed stars | $s_{(0)}$" | s(ξ)" | s(η)" | ξ" | η" | ξ" DTM | η" DTM | ξ" EGM2008 | η" EGM2008 | ξ" GOCE | η" GOCE |
|---|---|---|---|---|---|---|---|---|---|---|---|---|
| | | | | | | | **11.619** | **4.060** | **11.221** | **3.935** | **9.457** | **4.711** |
| HTL/15.07.2015 | 18 | 1.313 | 0.571 | 0.714 | 11.065 | 3.226 | 0.554 | 0.834 | 0.156 | 0.709 | -1.608 | 1.485 |
| | 9 | 1.190 | 0.738 | 0.911 | 11.268 | 3.261 | 0.351 | 0.799 | -0.047 | 0.674 | -1.811 | 1.450 |
| | 12 | 1.425 | 0.757 | 0.939 | 11.412 | 3.349 | 0.207 | 0.711 | -0.191 | 0.586 | -1.955 | 1.362 |
| HTL/13.07.2023 | 18 | 0.889 | 0.357 | 0.496 | 11.872 | 3.280 | -0.253 | 0.780 | -0.651 | 0.655 | -2.415 | 1.431 |
| | 8 | 0.815 | 0.486 | 0.692 | 11.909 | 3.244 | -0.290 | 0.816 | -0.688 | 0.691 | -2.452 | 1.467 |
| Max | | | | | 11.909 | 3.349 | | | | | | |
| Min | | | | | 11.065 | 3.226 | | | | | | |
| Max-Min | | | | | 0.844 | 0.123 | **Differences from the interpolated values and average** | | | | | |
| **Average** | | | | | **11.505** | **3.272** | **-0.114** | **-0.788** | **0.284** | **-0.663** | **2.048** | **-1.439** |
| Standard Deviation | | | | | 0.373 | 0.047 | | | | | | |
| | | | | | | | **11.301** | **3.725** | **10.947** | **3.384** | **9.637** | **4.277** |
| E/27-07-2015 | 19 | 2.692 | 1.079 | 1.479 | 10.208 | 2.486 | 1.093 | 1.239 | 0.739 | 0.898 | -0.751 | 1.791 |
| | 12 | 1.437 | 0.708 | 0.974 | 10.813 | 2.543 | 0.488 | 1.182 | 0.134 | 0.841 | -1.356 | 1.734 |
| | 10 | 2.971 | 1.586 | 2.353 | 10.732 | 2.603 | 0.569 | 1.122 | 0.215 | 0.781 | -1.275 | 1.674 |
| | 14 | 2.961 | 1.452 | 1.876 | 10.924 | 2.817 | 0.377 | 0.908 | 0.023 | 0.567 | -1.467 | 1.460 |
| E/24-07-2023 | 14 | 1.737 | 0.799 | 1.106 | 10.325 | 2.444 | 0.976 | 1.281 | 0.622 | 0.940 | -0.868 | 1.833 |
| | 7 | 1.869 | 1.216 | 1.731 | 10.795 | 2.021 | 0.506 | 1.704 | 0.152 | 1.363 | -1.338 | 2.256 |
| | 12 | 1.575 | 0.766 | 1.106 | 10.745 | 2.532 | 0.556 | 1.193 | 0.202 | 0.852 | -1.288 | 1.745 |
| Max | | | | | 10.924 | 2.817 | | | | | | |
| Min | | | | | 10.208 | 2.021 | | | | | | |
| Max-Min | | | | | 0.716 | 0.796 | **Differences from the interpolated values and average** | | | | | |
| **Average** | | | | | **10.649** | **2.492** | **-0.652** | **-1.233** | **-0.298** | **-0.892** | **1.012** | **-1.785** |
| Standard Deviation | | | | | 0.271 | 0.240 | | | | | | |
| | | | | | | | **10.769** | **4.038** | **10.646** | **3.957** | **9.978** | **4.127** |
| SE/30-07-2015 | 12 | 1.910 | 1.007 | 1.258 | 9.864 | 4.192 | 0.905 | -0.154 | 0.782 | -0.235 | 0.114 | -0.065 |
| | 9 | 1.768 | 1.030 | 1.370 | 10.138 | 3.513 | 0.631 | 0.525 | 0.508 | 0.444 | -0.160 | 0.614 |
| SE/28-07-2023 | 16 | 1.392 | 0.640 | 0.816 | 10.956 | 3.281 | -0.187 | 0.757 | -0.310 | 0.676 | -0.978 | 0.846 |
| | 8 | 1.441 | 0.938 | 1.195 | 11.033 | 3.327 | -0.264 | 0.711 | -0.387 | 0.630 | -1.055 | 0.800 |
| | 8 | 1.496 | 0.973 | 1.241 | 10.880 | 3.235 | -0.111 | 0.803 | -0.234 | 0.722 | -0.902 | 0.892 |
| Max | | | | | 11.033 | 4.192 | | | | | | |
| Min | | | | | 9.864 | 3.235 | | | | | | |
| Max-Min | | | | | 1.169 | 0.957 | **Differences from the interpolated values and average** | | | | | |
| **Average** | | | | | **10.574** | **3.510** | **-0.195** | **-0.529** | **-0.072** | **-0.448** | **0.596** | **-0.618** |
| Standard Deviation | | | | | 0.535 | 0.396 | | | | | | |
| | | | | | | | **11.759** | **4.364** | **11.015** | **4.379** | **9.644** | **4.742** |
| AIRA/11-07-2015 | 19 | 0.944 | 0.385 | 0.505 | 12.819 | 3.381 | -1.060 | 0.983 | -1.804 | 0.998 | -3.175 | 1.361 |
| | 9 | 0.993 | 0.596 | 0.778 | 12.657 | 3.312 | -0.898 | 1.052 | -1.642 | 1.067 | -3.013 | 1.430 |
| | 18 | 0.946 | 0.403 | 0.516 | 12.960 | 3.335 | -1.201 | 1.029 | -1.945 | 1.044 | -3.316 | 1.407 |
| | 7 | 0.778 | 0.482 | 0.715 | 12.227 | 4.017 | -0.468 | 0.347 | -1.212 | 0.362 | -2.583 | 0.725 |
| AIRA/12.07.2015 | 18 | 1.067 | 0.434 | 0.612 | 12.257 | 3.684 | -0.498 | 0.680 | -1.242 | 0.695 | -2.613 | 1.058 |
| | 11 | 1.219 | 0.622 | 0.907 | 12.390 | 3.834 | -0.631 | 0.530 | -1.375 | 0.545 | -2.746 | 0.908 |
| AIRA/20.06.2023 | 16 | 1.169 | 0.511 | 0.712 | 12.119 | 3.811 | -0.360 | 0.553 | -1.104 | 0.568 | -2.475 | 0.931 |
| AIRA/21.06.2023 | 16 | 1.053 | 0.429 | 0.682 | 12.073 | 3.174 | -0.314 | 1.190 | -1.058 | 1.205 | -2.429 | 1.568 |
| | 8 | 1.036 | 0.598 | 0.950 | 12.068 | 3.343 | -0.309 | 1.021 | -1.053 | 1.036 | -2.424 | 1.399 |
| AIRA/27.06.2023 | 19 | 0.707 | 0.294 | 0.389 | 12.722 | 3.158 | -0.963 | 1.206 | -1.707 | 1.221 | -3.078 | 1.584 |
| Max | | | | | 12.960 | 4.017 | | | | | | |
| Min | | | | | 12.068 | 3.158 | | | | | | |
| Max-Min | | | | | 0.892 | 0.859 | **Differences from the interpolated values and average** | | | | | |
| **Average** | | | | | **12.429** | **3.505** | **0.670** | **-0.859** | **1.414** | **-0.874** | **2.785** | **-1.237** |
| Standard Deviation | | | | | 0.333 | 0.304 | | | | | | |

potential (using GUT) and EGM2008 global model, after a methodology described in detail in (Bădescu, O., et al, 2016b), by interpolation.

For the astronomical vertical deviation, geodetic coordinates are referred to ellipsoid GRS80 – ETRS89 (Geodetic Reference System 1980 – European Terrestrial Reference System 1989).

Related to the astrometric reductions, we mention that:

- The star catalogue used in the astrometric reductions was FK6 (Sixth Catalogue of Fundamental Stars);
- Astrometric reductions from J2000.0 catalogue epoch to observations epoch were done using a software based on NOVAS package of subroutines and functions (Naval Observatory Vector Astrometry Software, Version 3.1 Fortran, C, and Python Editions, http://aa.usno.navy.mil/software/novas/)
- Astrometric reductions were verified with MICA v.2.2.2 software application (Multiyear Interactive Computer Almanac, http://aa.usno.navy.mil/software/mica/);

Values of vertical deviation components incorporate the correction of the polar motion.

## 5. REMARKS AND CONCLUSIONS

In total, we achieved 11 observations' nights, in 4 different stations and 2 different years, 2015 and 2023, that means an interval of 8 years. In 3 stations were made 2 nights of observations, both in 2015 and in 2023. In 1 station (AIRA) were effectuated 2 nights of observations in 2015 and 3 in 2023. On the whole, in all 4 stations, were obtained 27 determinations of vertical deviations from which 15 in 2015 and 12 in 2023. 5 determinations were made at HTL station (from which 2 in 2023), 7 at E station (from which 3 in 2023), 5 at SE station (from which 3 in 2023), and 10 at station AIRA (from which 4 in 2023). The total number of the used stars in determinations, separately 2015 and 2023, is depicted in Figure 7.

For all station and for all observations sessions, were recorded the parameters fitrms, separately in azimuth and zenithal distance. The software calculates the centroid of the brightest object from every image using a bi-dimensional circular Gaussian function. Precision of the centroid detection is about of 1/20 pixel in the case of stars with detection sigma bigger than 5. Based on centroids, then is calculated, separately or simultaneous, times of intersections with the two axes (virtual reticular wires) using a function of order II for fitting. Also, it is providing the image of the calculated trajectory (Figure 5) and root mean square (rms) of the fitting – fitrms (see Explanation at Table 1, (7), (10)). Figure 8 shows the average of the fitrms obtained in station AIRA, in 2023, separately for azimuth (A) and zenithal distance (Z). Figure 9 shows the average number of images captured for every observation night (the total number of captured images into a single night divided by the total number of the observed stars) and the total number of imaged captured into a single night, in station AIRA, in 2023.

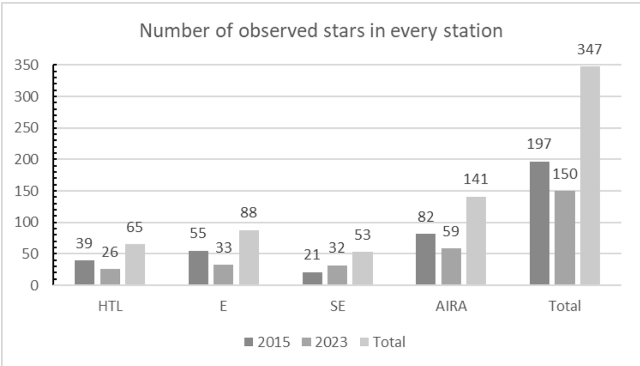


Fig. 7 – Number of observed stars in every station (HTL, E, SE and AIRA) as well as the total number of observed stars, separately on 2015 and 2023. It should be mentioned that a single star or more can be found in several observation sessions from different stations or in different years.

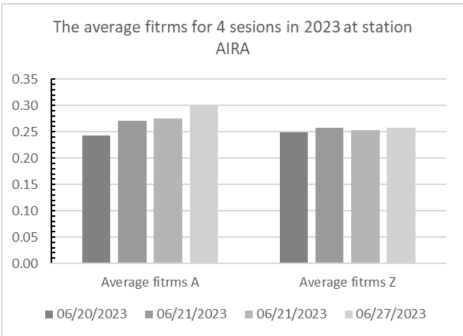


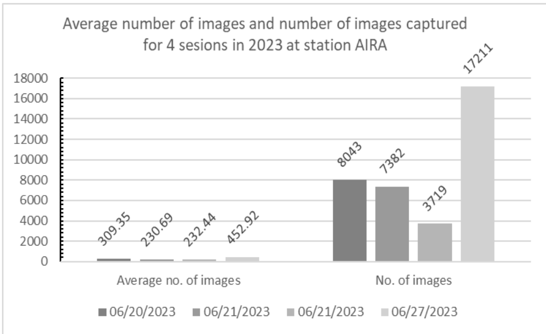


Fig. 8 – Average fitrms in azimuth (A) and zenithal distance (Z), AIRA 2023.

Fig. 9 – Average no. of captured images for for every observation night and the total no. of the observed stars.

Figure 10 shows the results obtained, separately for both components of the vertical deviation and all 4 stations (HTL, E, SE, AIRA), from CCD astro-geodetic measurements, and similar values extracted from models (DTM, EGM2008, GOCE) by interpolation.

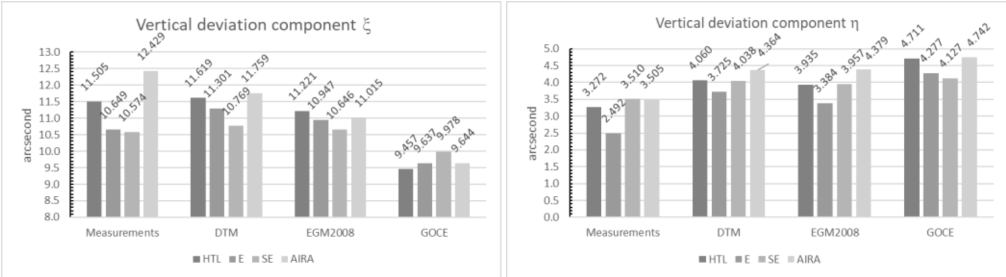


Fig. 10 – Vertical deviation components in all 4 stations from in-situ measurements and models (by interpolation).

Figure 11 shows the individual standard deviation resulted from measurements, for every session of observations, separately by components: $s_{(0)}$ standard deviation of a single series; $s_{(\xi)}$ standard deviation of the meridian component $\xi$, $s_{(\eta)}$ standard deviation of the prime vertical component $\eta$, all values expressed in arcseconds.

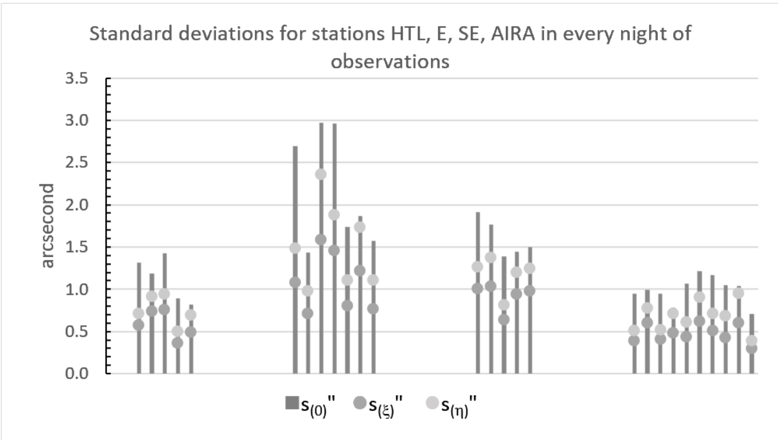


Fig. 11 – Individual standard deviation resulted from functional stochastic model in all 4 stations (also, see the Table 2).

Differences between our results and values extracted from DTM model are under 1 arcsec with a single exception at the station E, for the $\eta$ component (−1.233 arcsec). The station E was a problematic station, taking into account the largest individual standard deviation obtained, although the measurements were performed in the same way in all stations. It should also be said that the E station is relatively close to the intensively traveled ring road of Bucharest even at night, the road being parallel to an electrified railway line (25 m to the railway and 75 m to the road). However, the values extracted by interpolation from the DTM model are very valuable for comparisons because it is based exclusively on astro-geodetic (historical) determinations.

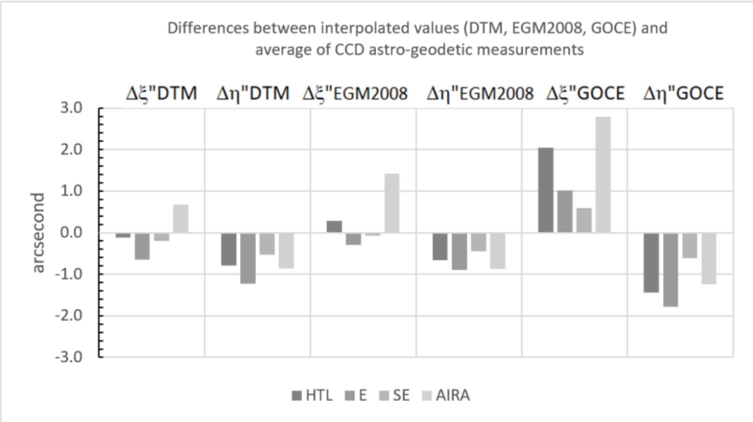


Fig. 12 – Differences between our determinations and used models DTM, EGM2008 and GOCE, separately by components $\xi$ and $\eta$.

Differences between our results and values extracted from EGM2008 model also are under 1 arcsec with a single exception at the station AIRA, for the $\xi$ component (+1.414 arcsec). There is an acceptable agreement with EGM2008 global model, approximatively arc-second, in accordance with results obtained in other studies (Featherstone W.E. and Morgan L., 2007; Hirt C., et al., 2010b; Voigt, C. and Denker, H., 2011; Pavlis N.K., et al., 2012).

The worst results were obtained in comparison with vertical deviations derived from GOCE global model. The agreement between CCD astro-geodetic deviations and deviations derived from GOCE exceeds the values obtained in other studies. A study already started (Gornea, A.I., et al, 2017), and future work will be done to clarify the problem.

We consider that the results obtained are promising, especially with the long temporal distance between data of acquisitions (2015, 2023). Future work will focus on achieving a more consistent program of observations/measurements, densifying the number of astro-geodetic stations and making at the same time a consistent statistical evaluation of the results obtained.

*Acknowledgements.* This work was supported by a grant of the Ministry of Research, Innovation and Digitization, CCCDI-UEFISCDI, project number PN-III-P2-2.1-PED-2021-1789, within PNCDI III.

## REFERENCES


Bădescu, O., Nedelcu, D.A., Călin, A., Dumitru, P.D., Plopeanu, M., Popescu, M.: 2015, Mobile platform for new astro-geodetic observations, Romanian Astron. J. **25**, 63-73.

Bădescu, O., Nedelcu, D.A., Călin, A., Dumitru, P.D., Călin, L., Popescu, M.: 2016a, Astro-geodetic platform for high accuracy geoid determination. Romanian Astron. J. **26**, 57–65.

Bădescu, O., Dumitru, P.D., Călin, A., Nedelcu, D.A.: 2016b, Case study regarding the determination and use of the astro-geodetic deviations of the vertical in Romania, Environmental Engineering and Management Journal **15**.

Bădescu, O., Plopeanu, M., Nedelcu, A., Popescu, P., Paraschiv, P.: 2010, A project for modern astrogeodetic geoid determination, Romanian Astron. J. **20**, 79-84.

Bürki, B., Somieski, A.E., Sorber, P., H.G. Kahle, Hirt, C.: 2007, The Digital Astronomical Deflection Measuring System (DIADEM), In: Swiss National Report on the Geodetic Activities in the years 2003-2007, presented to the XXIV General Assembly of the IUGG in Perugia, Italy, ISBN 978-3- 908440-15-4, Swiss Geodetic Commission, 143-144.

Călin A., Bădescu O., Dumitru P.D., Nedelcu D.A., Savu, A.: 2018, Tests regarding determinations of the vertical deviation by a new CCD astro-geodetic procedure, 17th edition International Technical-Scientific Conference Modern Technologies for the 3rd Millennium, March 22-23, Oradea (Romania).

Featherstone, W.E., Morgan, L.: 2007, Validation of the AUSGeoid98 model in Western Australia using historic astrogeodetically observed deviations of the vertical, Journal of the Royal Society of Western Australia, **90**, 143-150.

Gornea, A.I., Nedelcu, D.A., Dumitru, P.D.: 2017, Some results regarding statistical evaluation of the CCD astro-geodetic vertical deviation, Romanian Astron. J., **27**, 99–106.

GUT (GOCE User Toolbox): 2014, GUT User Guide and Algorithm Descriptions, European Space Agency (ESA), ESA-GUT-AD-001, v.2.2.

Hirt, C., Bürki, B.: 2002, The Digital Zenith Camera - A New High-Precision and Economic Astrogeodetic Observation System for Real-Time Measurement of Deflections of the Vertical, in Tziavos, I. (ed), 3rd Meeting of the International Gravity and Geoid Commission, Aug. 26, 161-166. Thessaloniki, Greece.

Hirt, C. and Reese, B.: 2004, High-Precision Astrogeodetic Determination of a Local Geoid Profile Using the Digital Zenith Camera System TZK2-D, Electronic Proc. IAG GGSM2004, IAG International Symposium Porto, Portugal.

Hirt, C., Bürki, B., Somieski, A., Seeber, G.: 2010a, Modern Determination of vertical deflections using digital zenith cameras, Journal Surveying Engineering **136**(1), 1-12.

Hirt C., Marti U., Bürki B., Featherstone W.E.: 2010b, Assessment of EGM2008 in Europe using accurate astrogeodetic vertical deflections and omission error estimates from SRTM/DTM2006.0 residual terrain model data, Journal of Geophysical Research: Solid Earth, **115**, B10.

Jekeli, C.: 1999, An analysis of vertical deflections derived from high-degree spherical harmonic models, Journal of Geodesy, 73, 10-22.

Pavlis, N.K., Holmes, S.A., Kenyon, S.C., Factor, J.K.: 2012, The development and evaluation of the Earth Gravitational Model 2008 (EGM2008), Journal of Geophysical Research, 117, B04406, doi:10.1029/2011JB008916.

Voigt, C., Denker, H.: 2011, Validation of GOCE Gravity Field Models by Astrogeodetic Vertical Deflections in Germany, Proceedings of the 4th International GOCE User Workshop, Munich, 31 March – 01 April, ESA Special Publication SP-696.


*Received on 4 December 2023*